Front. Optoelectron. China 2008, 1(3–4): 247–257
DOI 10.1007/s12200-008-0034-0

RESEARCH ARTICLE

Analyses and calculations of noise in optical coherence tomography systems

Xiaonong ZHU (✉)[1], Yanmei LIANG[1], Youxin MAO[2], Yaqing JIA[1], Yiheng LIU[1], Guoguang MU[1]

1 Institute of Modern Optics, Nankai University, Key Laboratory of Opto-electronic Information Science and Technology, Ministry of Education, Tianjin 300071, China
2 Institute for Microstructural Science, National Research Council Canada, Ottawa, ON, K1A 0R6, Canada

Abstract Significant progress has been made in the study of optical coherence tomography (OCT) — a non-invasive, high resolution, and *in vivo* diagnostic method for medical imaging applications. In this paper, the principles of noise analyses for OCT systems have been described. Comparisons are made of signal-to-noise ratios for both balanced and unbalanced detection schemes under the ideal no-stray light situation as well as the non-ideal situation where residual reflections and scatterings are presented. Numerical examples of noise calculation accompanied by detailed comparison of the main characteristics of both time-domain and frequency-domain OCT systems are also presented. It is shown that a larger dynamic range can be achieved for a Fourier-domain OCT system even under the circumstances of high-speed image acquisition. The main results presented in this paper should be useful for the development of high performance OCT systems.

Keywords optical coherence tomography (OCT), noise analyses, sensitivity, signal-to-noise ratio (SNR)

1 Introduction

As an advanced high precision medical imaging method, optical coherence tomography (OCT) is the latest development of the technologies in optical tomography [1–3]. By making use of the low coherence of a broadband light source, OCT detects the scattered light originated at different depths of a biological tissue, and from these signals of different depth, topographical image information of the sample of interest is obtained and rendered. OCT is capable of accurately mapping out the size, shape, and location of the area of plausible pathological changes. Different from traditional ultrasonic technology and computer tomography (CT), OCT has the great advantage of higher spatial resolution and greater detection sensitivity. The resolution of an OCT system can be close to that of the commonly used biopsy method. Compared with the various diagnostic approaches used in tissue pathology, OCT is advanced in its employment of non-contact and compact detection head so that it can be used for *in vivo* and non-invasive diagnoses, and in some cases to replace the biopsy of living organisms. All these important features make it possible for OCT to be adopted in many areas where the means of tissue pathology cannot be easily applied such as inspection of blood vessels, *in situ* monitoring of micro surgery and its recovering process, etc. Therefore, OCT is also called optical biopsy. It is believed that OCT may play a significant role in the future in reducing or avoiding the false negative results of diagnoses of cancers.

A typical OCT system normally includes a broadband light source, an optical Michelson interferometer, an optical beam scanning unit, a weak signal collection circuit, and certain image processing and display software. With the continuous development of OCT technologies, various OCT systems tailored for a specific functionality have been developed, such as polarization-sensitive OCT [4,5], Doppler OCT [6,7], differential absorption OCT [8], Fourier-domain OCT [9], etc. All these OCT systems may be classified into two main categories, namely, time-domain OCT (TD-OCT) and frequency-domain OCT (FD-OCT). For the time-domain OCT, the longitudinal scan or A-scan is realized through the fast variation of an optical delay line [10], whereas for the frequency-domain OCT, the depth information is obtained through measuring the optical spectrum of interference signal and performing the fast Fourier transform, with no direct A-scan being involved [11,12].

Presently, how to increase the detection depth, how to raise the detection speed and how to improve the signal to

Translated and revised from *Acta Photonica Sinica*, 2007, 36(3): 452–461 [译自: 光子学报]

E-mail: xnzhu1@nankai.edu.cn

noise ratio represent three key areas in studies of OCT technologies. These subjects are actually not independent. For example, the maximum detection depth is related to the dynamic range, and the dynamic range is linked to the detection speed and the system noise. Because in almost all OCT systems detection of very weak signal from backward scattering is involved and every part in an OCT instrument may severely affect the noise performance of the entire system, it is critical to carefully examine the characteristics of various noises in OCT detection in order to obtain high quality tomographic images.

In this paper, the system noise presented in OCT systems shall be systematically described and analyzed, with a goal of designing and developing a high-performance, practical OCT instrument. We present the basic principles of noise calculations, comparison of noise characteristics and the corresponding calculation formulae for both ideal (without stray light) and non-ideal (with stray light), balanced and unbalanced detection schemes, and show the calculated results of typical noise and sensitivity of both time-domain and frequency-domain OCT systems under the shot noise limit.

2 Noise of OCT systems

As the longitudinal coherence gating signal of an OCT system is obtained from a two-beam optical interference setup, such as the Michelson interferometer, the signal, I_P, detected by the photoelectric detector follows the typical principle of two-wave interference, namely

$$I_P(\Delta l) = I_S + I_R + 2\sqrt{I_S I_R}|\tau_{SR}(\Delta l)|\cos(k_0\Delta l + \alpha_{SR}), \quad (1)$$

where, Δl is the optical path difference between the signal beam coming from the sample and the reference beam reflected by a mirror; I_S, I_R are the respective optical intensities of these two beams; $\tau_{SR}(\Delta l)$ is the normalized complex cross-correlation function of the two beams; k_0 is the wave number, and α_{SR} is the initial constant phase difference between the two beams. What detected in OCT systems are the magnitudes of $2(I_S I_R)^{1/2}|\tau_{SR}(0)|$ associated with different sample depths. If the scattering process inside a sample is completely linear, and no spectral modulation exists on the incident beam, $\tau_{SR}(\Delta l)$ will be the first-order auto-correlation function or Fourier transform (FT) of the spectral density of the light source. In general, light scattering in OCT systems is a linear process with a certain amount of spectral-modulation, which means that the interference signal will be the convolution between the auto-correlation function of the light source and the impulse response of the biological sample [3].

$|\tau_{SR}(\Delta l)|$ may be regarded as the longitudinal point spread function of an OCT imaging system, which determines the longitudinal resolution of the OCT system. The lateral resolution of an OCT system is related to the wavelength of the light source and the effective numerical aperture (NA) or the degree of light convergence on the sample. By laterally scanning the light beam in parallel to the sample surface, or translating the sample in reference with the detection beam, a two-dimensional transect image of the sample can be obtained. Similar to the weak signal detection technique of electronics based on the heterodyne detection scheme, an OCT system may be taken as an optical heterodyne detection system where the reference beam plays the role of a local oscillator. Therefore, some important characteristics of the conventional heterodyne detection technique, such as anti-interference, high sensitivity, etc., will also apply to OCT systems.

The signal-to-noise ratio (SNR) of an OCT system can be defined in two different ways. One definition is the square of the ratio of i_g to σ_i:

$$\mathrm{SNR} = \left(\frac{i_g}{\sigma_i}\right)^2, \quad (2)$$

where i_g is the detected signal current after the photoelectric transformation; σ_i is the statistical deviation or the root mean square (RMS) of the background noise current without the presence of any signal. The other definition of SNR is the ratio of 100% back-scattering rate from a perfectly reflecting sample to the minimum scattering rate that is just detectable [3], i.e.,

$$\mathrm{SNR} = \frac{1}{R_{min}}, \quad (3)$$

where the minimum scattering rate relates to the situation that the signal power of sample scattering equals to the noise power of the system. It is worthwhile to point out that, in practice, either Eq. (2) or Eq. (3) is given in the form of a logarithm, namely, $\mathrm{SNR} = 10\lg(i_g/\sigma_i)^2$ or $\mathrm{SNR} = 10\lg(1/R_{min})$. If SNR is equal to 100 dB, it means that the dynamic range of the optical power is 1×10^{10}, but the dynamic range of the current is 1×10^5.

From Eq. (1), the peak value of photoelectric current generated by the interference term can be expressed by

$$i_g = \frac{\eta e}{h v_0}\sqrt{2P_R P_S}, \quad (4)$$

where η is the quantum efficiency of the detector, e is the electronic charge, h is the Planck's constant, v_0 is the mean frequency of the incident light, P_R, P_S are the optical powers detected by the photoelectric detector respectively from the reference arm and sample arm, which are also the corresponding integrations of I_R, I_S given by Eq. (1) over the sensitive area of the detector. The statistical deviation or the RMS of the noise current, σ_i, can be generally described by

$$\sigma_i^2 \equiv \langle \Delta i_i^2 \rangle = \langle \Delta i_{sh}^2 \rangle + \langle \Delta i_{ex}^2 \rangle + \langle \Delta i_{re}^2 \rangle + \langle \Delta i_f^2 \rangle, \quad (5)$$

where the shot noise, $\langle \Delta i_{sh}^2 \rangle$, the excess intensity noise, $\langle \Delta i_{ex}^2 \rangle$, the thermal noise, $\langle \Delta i_{re}^2 \rangle$, and the flicker noise, $\langle \Delta i_f^2 \rangle$, are respectively determined by

$$\langle \Delta i_{sh}^2 \rangle = 2e\langle i \rangle B, \quad (6)$$

$$\langle \Delta i_{ex}^2 \rangle = \frac{2}{3}\frac{(1+V^2)\langle i \rangle^2 B}{\Delta v}, \quad (7)$$

$$\langle \Delta i_{re}^2 \rangle = \frac{4k_B TB}{R_L}, \quad (8)$$

$$\langle \Delta i_f^2 \rangle \propto \frac{1}{f}. \quad (9)$$

In the above expressions, the brackets denote the ensemble average, $\langle i \rangle$ is the average photocurrent of the detector, B is the electrical bandwidth of the detection system, V is the polarization ratio of the light source, Δv is the frequency full-width at half-maximum (FWHM) of the light source, k_B is the Boltzmann's constant, T is the absolute temperature, R_L is the equivalent load resistance of the detection circuit.

Shot noise or quantum noise originates from the random arrival of photons at the photodetector, corresponding to the quantum fluctuation. The excess intensity noise is due to the instability of the incident light associated with the random summation of different frequency components of the broadband light source. The excess intensity noise is also called the random beat frequency noise. In deriving Eq. (7), it is assumed that the spectrum of the light source has a Gaussian profile. For other spectral distributions, $3\Delta v/2$ in Eq. (7) should be replaced by an effective frequency bandwidth [3]. Thermal noise, or receiver noise, comes from the random thermal motion of electrons inside a medium when there is no incident light. Flicker noise represents the noise caused by the random variation of the environment, which in general decays rapidly as frequency increases, following the rule of $1/f$. For OCT systems, the interference signal term has a relatively high carrier frequency (often larger than several kHz), and therefore the flicker noise can be ignored.

Substituting Eqs. (4)–(8) into Eq. (2), assuming $\alpha \equiv \eta e/(hv_0)$ and $\langle i \rangle$ is mainly from the reference light, so that $\langle i \rangle = \eta e P_R/(hv_0)$, we obtain

$$\mathrm{SNR} = \frac{\alpha^2 P_R P_S}{\left(\frac{2k_B T}{R_L} + e\alpha P_R + \frac{(1+V^2)(\alpha P_R)^2}{3\Delta v}\right)B}. \quad (10)$$

3 Time-domain and frequency-domain OCT systems

The schematics of the time-domain and the spectral-domain OCT systems are shown in Figs. 1(a) and 1(b) respectively. For time-domain OCT systems, the length of the reference arm is varied rapidly in order to detect the signal from different depths of the sample. In this case, I_P in Eq. (1) will be a function of time. With V_R representing the scanning speed of the group delay in the reference arm, we have $\Delta l = 2V_R t$. By substituting Δl into Eq. (1), we obtain that the carrier frequency of a time-domain OCT system f_0 is equal to $2V_R/\lambda_0$, where λ_0 is the center wavelength of the light source. Apparently, the signal frequency bandwidth Δf is given by $\Delta f = 2V_R\Delta\lambda/\lambda_0^2 + 2\Delta V_R/\lambda_0$. If V_R is a constant, we obtain $\Delta f/f_0 = \Delta\lambda/\lambda_0$.

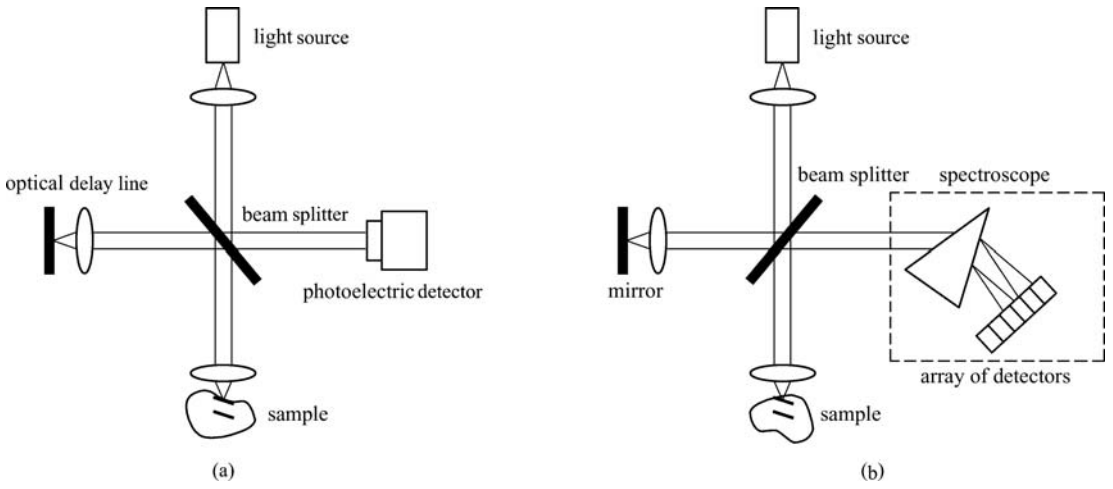

Fig. 1 Schematics of optical layouts. (a) Time-domain OCT systems; (b) frequency-domain OCT systems

For spectral-domain OCT systems, the spectrum of the interference signal is measured directly, and the information of different depths of the sample is derived by performing an inverse fast Fourier transform (IFFT) of the measured spectrum. In this case, without the reference arm constantly scanning back and forth, the spectral interferogram intensity is the result of interference between the scattering light from different depths of the sample and the reference light. The principle of the spectral-domain OCT is equivalent to a reversed process of a Fourier transform spectrometer, namely, the wave number and the depth form a Fourier transform pair. The spectral width determines the longitudinal resolution, and the spectral resolution confines the maximum detectable depth of the scattering signal.

Because the time-domain and the frequency-domain OCT systems use totally different approaches in realizing A-scan, their signal detection and processing methods are also different, and the noise characteristics of these two types of OCT systems are not the same. We will present detailed discussions on the noise characteristics of time-domain OCT systems in Sections 4 and 5, and make further noise analyses with calculation examples for frequency-domain OCT systems in Sect. 6.

4 Analysis of noise in time-domain OCT systems

From Eq. (10), we can see that SNR in OCT systems is directly proportional to the optical power of scattered light from the sample, P_S, and inversely proportional to the frequency bandwidth of the opto-electric signal, and moreover, a relatively complex relationship exists between SNR and the optical power of the reference beam, P_R. In general, there are three extreme cases of SNR in time-domain OCT systems, which are

(a) Limit of thermal noise:

$$\mathrm{SNR} = \frac{2\alpha^2 P_R P_S}{k_B T}\frac{R_L}{B}. \tag{11}$$

This case corresponds to the situation where either the source power is very low, or the reflection from the reference arm is noticeably weak, or the noise of the detector is rather large.

(b) Limit of shot noise:

$$\mathrm{SNR} = \frac{\alpha P_S}{eB}. \tag{12}$$

Under this extreme situation, SNR of OCT systems is proportional to the signal power only, i.e., it has a linear relationship with the optical power of light source, and does not depend on the power of the reference light beam. This normally represents the optimum operation window for OCT systems.

(c) Limit of redundancy intensity noise:

$$\mathrm{SNR} = \frac{P_S}{(1+V^2)P_R}\frac{3\Delta v}{B}. \tag{13}$$

This limit corresponds to the case where the optical power received by the detector is too high. In this situation, increasing the power of the light source cannot improve SNR, while on the contrary, decreasing the power of the reference beam may help to improve the system SNR. In addition, another special feature of the redundancy intensity noise limit is that SNR is directly proportional to the frequency bandwidth of the detection system. The wider the frequency bandwidth, the larger the SNR would be. Since both P_S and P_R are proportional to the incident optical power, SNR determined by Eq. (13) is essentially independent of the intensity of the incident light, which essentially represents the situations where SNR is saturated because the incident optical power approaches infinity.

Now, let us estimate the SNR values for an actual OCT system. We assume that the center wavelength of the light source, λ_0, is 1.5 μm; its output power, P, is 10 mW; spectral bandwidth, $\Delta\lambda$, is 80 nm; polarization ratio, V, equals to 1; the quantum efficiency of the photo-electric detector, η, is 0.65; the equivalent load, R_L, is 1 kΩ; the temperature, T, is 300 K; and the frequency bandwidth of the optoelectric signal, B, is 100 kHz. We further assume that the optical power of the reference beam, P_R, is 1 mW, i.e., it is one tenth of the source power. By substituting these numbers into Eqs. (6)–(8) respectively, we obtain the RMS currents associated with the three different types of noise: 4.6×10^{-9} A for shot noise, 7.3×10^{-8} A for redundancy intensity noise, and 1.3×10^{-9} A for thermal noise. The corresponding minimum detectable power is 4.3×10^{-12} W (SNR = 1). Suppose the maximum signal power is 1 mW, the detected total photo-electric current will be 1.1×10^{-3} A. From Eq. (10), we get SNR ≈ 84 dB for this OCT system.

If an OCT system is operated under the shot noise limit, and in the meantime the bandwidth, Δf, and the carrier frequency f_0 of the interference signal meet with the relationship $\Delta f/f_0 = \Delta\lambda/\lambda_0$, where $\Delta\lambda$ and λ_0 are the spectral bandwidth and center wavelength of the light source, we can then obtain from Eq. (12) and using $B = 2\Delta f$,

$$\mathrm{SNR} = \frac{\alpha P_S \lambda_0}{2e\Delta\lambda f_0} = \frac{\alpha P_S \lambda_0^2}{4e\Delta\lambda V_R}, \tag{14}$$

where $V_R = (\lambda_0/2)f_0$ represents the group delay scan speed of the reference arm.

From Eq. (14), it can be seen that, in this case, the SNR of the OCT system is directly proportional to the square of the central wavelength and the power of the light source, and inversely proportional to the spectral bandwidth and the group delay scan speed.

Because the longitudinal resolution of time-domain OCT systems is inversely proportional to the coherence length of the light source ($l_c \propto \lambda_0^2/\Delta\lambda$), Eq. (14) implies that requirement of high SNR is in conflict with the great longitudinal resolution and high image capturing speed. Therefore, a compromise among these parameters must be considered. Using the values of the parameters shown above, and $V_R = 4$ m/s, $P_S = 1$ mW, we can readily obtain SNR = 99.4 dB from Eq. (14). If V_R is increased ten times, namely, $V_R = 40$ m/s, then SNR will be decreased to 89.4 dB.

Equation (14) tells us that in shot noise limit, for a given image grid number SNR will have a 3 dB decrease when the imaging capturing speed is doubled. In other words, if we want to keep the same SNR, the incident light intensity should be doubled when we double the image capturing speed.

Figure 2 shows the variation of SNR of the example time-domain OCT system versus the power of the reference light calculated from Eq. (10). Assuming the center wavelength of light source $\lambda_0 = 1.5$ μm, spectrum bandwidth $\Delta\lambda = 80$ nm, signal power $P_S = 1$ mW, polarization ratio $V = 1$, quantum efficiency of the photoelectric detector $\eta = 0.65$ A/W, effective load of the detection circuit $R_L = 1$ kΩ, temperature $T = 300$ K, and a frequency bandwidth of the electric signal $B = 100$ kHz. Also shown in Fig. 2 are the SNR values for the three extreme situations. From the respective traces in Fig. 2, it is clear that the SNR is independent of the power of the reference light at shot noise limit, directly proportional to the power of the reference light at thermal noise limit, and when the redundancy intensity noise is dominant, the higher the power of the reference light, the lower the SNR. Also, from the plot in Fig. 2, it can be clearly seen that for an OCT system that is not operated at any of the three noise limits, an optimum reference light power exists. By differentiating SNR with respect to P_R in Eq. (10), the expression of the optimum of P_R can be easily obtained as

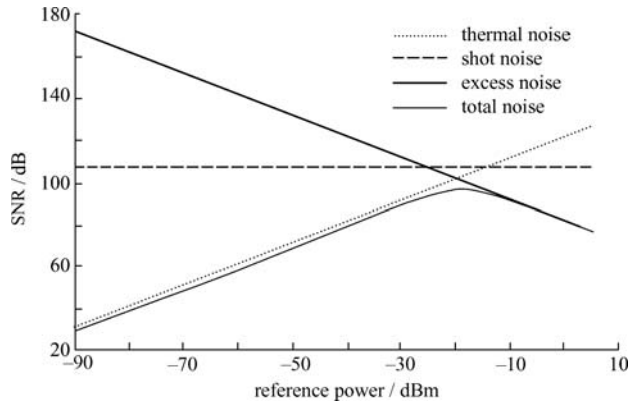

Fig. 2 Variation of SNR versus the power of reference light for a time-domain OCT system

$$(P_R)_{Opt} = \sqrt{\frac{k_B T}{R_L}\frac{3\Delta v}{(1+V^2)\alpha^2}}. \tag{15}$$

It should be noticed that the optimum of P_R does not depend on the intensity of the signal light. Substituting the values we used in the examples given above into Eq. (15), we get $(P_R)_{Opt} = 0.01$ mW. This number is consistent with the corresponding result in Fig. 2. From the lower trace (total noise line) in Fig. 2, we can see that SNR reaches a maximum of 98 dB for $P_R = -20$ dBm. For comparison, if $P_R = 1$ mW, we have SNR = 82 dB. The importance of having an optimized P_R is thus apparent.

5 Further discussion on noise characteristics of time-domain OCT systems

In this section, we shall make some further analyses of several important noise-related problems encountered in designing an actual OCT system.

5.1 Minimum detectable power of signal light

Among many existing literatures on OCT systems, sensitivity and SNR are commonly treated as the same thing. However, as we all know, the SNR defined by Eq. (10) actually only provides a relative dynamic range of an OCT system, and it does not tell us what the minimum detectable signal power is in absolute sense. If we set SNR = 1 in Eq. (10), the minimum detectable power of signal light or sensitivity can be derived as

$$\beta_{sensitivity} \equiv (P_S)_{min} = \frac{\left(\frac{2k_B T}{R_L} + e\alpha P_R + \frac{(1+V^2)(\alpha P_R)^2}{3\Delta v}\right)B}{\alpha^2 P_R}. \tag{16}$$

At the limit of shot noise, we have

$$(P_S)_{min} = \frac{h v_0 B}{\eta}. \tag{17}$$

Substituting into Eq. (17) the parameters of $B = 100$ kHz and $\eta = 0.65$ for the 1.5 μm OCT system described above leads to $(P_S)_{min} = 2.04 \times 10^{-14}$ W. This is only an ideal result. In practice, whether such sensitivity can be achieved or not will depend on the performance of the photoelectric detector and the detection circuit. The maximum dynamic rang of an OCT system may be calculated with $(P_S)_{min}$ and the maximum saturation light power P_{sat} of the photodetector. Suppose $P_{sat} = 1$ mW, then the maximum dynamic range for the OCT system we just discussed will be $10\lg[P_{sat}/(P_S)_{min}]$ dB = 107 dB.

Eq. (17) also indicates that as a result of two-beam interference measurement the noise equivalent power (NEP) of an OCT system is half of that of the same detector under a non-heterodyne detection scheme [13]. Suppose the dark current of the photodetector is $i_D = 1$ nA, then the NEP of the dark current will be given by

$$\mathrm{NEP}_D = \frac{h\nu_0}{\eta e} i_D. \tag{18}$$

Using the same values of the parameters we used above, we have $\mathrm{NEP}_D = 6.4 \times 10^{-10}$ W. We can thus see that $(P_S)_{\min} \ll \mathrm{NEP}_D$.

5.2 Balanced and unbalanced heterodyne detections

Depending on whether one detector is used to perform, one channel detection or two detectors are used for two channel detection together with a differential amplifier. OCT systems can be divided into two categories: balanced heterodyne detection and unbalanced heterodyne detection. Figure 3 shows three different schematics of balanced heterodyne detection. Usually, for balanced heterodyne detection, two beams of equal average power are detected separately by two different detectors D1 and D2, and a π phase difference exists in the two sets of interference signals. Through differential amplification, the background signals from the two channels cancel each other out, whereas the respective interference signal is enhanced, and, only the resultant interference signal is processed in the succeeding signal processing.

From Fig. 3, it can be seen that the third scheme has a very simple but rather efficient structure because of the use of an optical circular. Detailed analysis of the noise present in this type of OCT systems may be found in Ref. [14].

It is worth mentioning that the simplest Michelson interferometer shown in Fig. 1(a) belongs to the unbalanced heterodyne detection category. In this case, the photodetector receives not only the interference signal, but also the direct current (DC) background signal described by the first two items in Eq. (1). Because the DC background signal also contains intensity fluctuation noise, instead of being purely direct current, its presence will affect the noise characteristics of the whole system [15]. Further studies of the noise characteristics of both balanced and unbalanced heterodyne detection systems may benefit from noise analysis theories of optical low coherence reflectometry (OLCR), which has been widely adopted in the field of optical communications [16].

5.3 System noise under non-ideal situations

In the analyses given above, only the signal light from the sample arm and the reference light from the reference arm are considered. That means we have only taken the noise within the signal and reference light into account. In deriving Eq. (10), another hypothesis is also made, namely, the optoelectronic current is only affected by the reference light. But for a real-world OCT system, other stray lights and residual reflections from various surfaces or interfaces are certainly presented. That is to say, the total mean optical current for a real OCT system should be composed of three parts as

$$\langle i \rangle = \langle i_R \rangle + \langle i_S \rangle + \langle i_N \rangle, \tag{19}$$

where $\langle i_R \rangle$ and $\langle i_S \rangle$ are the mean optical current caused

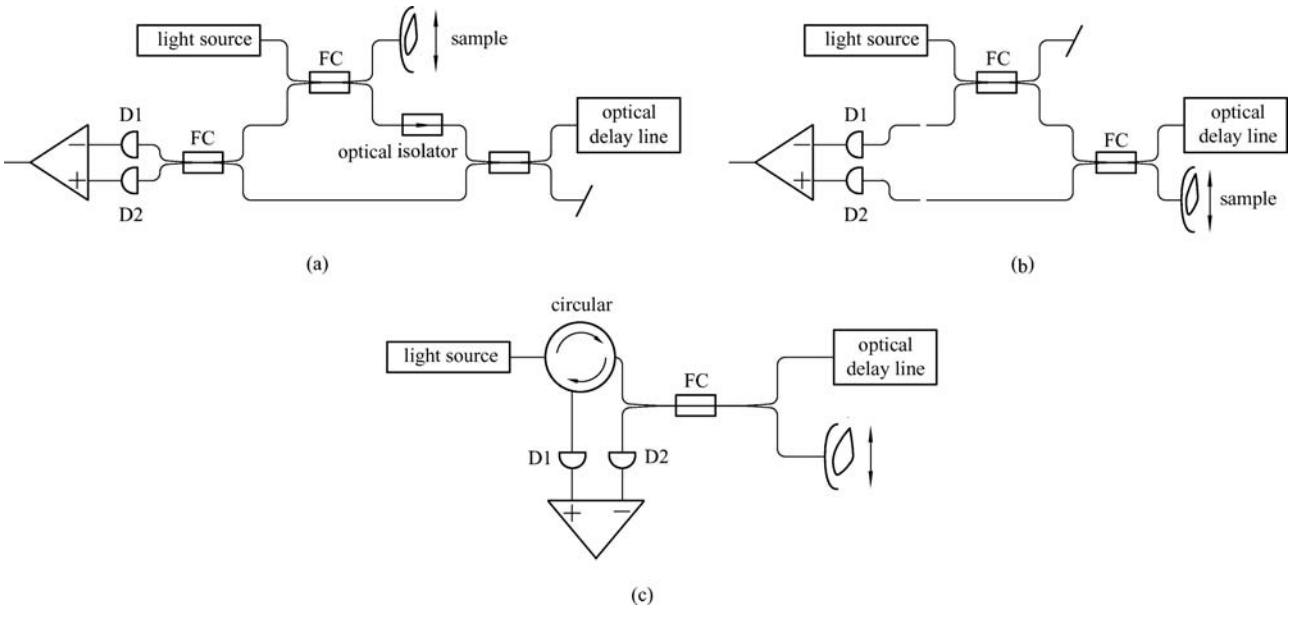

Fig. 3 Three different schematics of balanced heterodyne detection (FC: fiber coupler; D1, D2: detector)

by the reference light and signal light respectively, and $\langle i_N \rangle$ is the mean optical current caused by other stray lights. Apparently, each of these three terms will have its own intensity fluctuation noise (or beat noise) described by $b\langle i_m \rangle^2/\Delta v$ (subscript $m = R, S, N$) and the beat noise among them: $b\langle i_m \rangle\langle i_q \rangle/\Delta v$, $m \neq q$ (m, $q = R, S, N$). Coefficient b is related to the polarization of the light and its spectral density [16]. By substituting Eq. (19) into Eqs. (6) and (7), and substituting the results into Eq. (5), a more universal expression of the spectral density of the optical current of an OCT system can be obtained as

$$\frac{\langle \Delta i_i^2 \rangle}{B} = \frac{4k_B T}{R_L} + 2e(\langle i_R \rangle + \langle i_S \rangle + \langle i_N \rangle) + \frac{2(1+V^2)}{3\Delta v}(\langle i_R \rangle + \langle i_S \rangle + \langle i_N \rangle)^2. \quad (20)$$

Under the conditions of $\langle i_N \rangle = 0$ and $\langle i \rangle \approx \langle i_R \rangle$, the simplified SNR expression given by Eq. (10) can be derived from Eq. (20). That means, since in Eq. (10), $\langle i \rangle^2 \approx \langle i_R \rangle^2$ is used, it not only implies the condition of unbalanced detection, but also omits the contributions from the frequency beat as well as the signal light to the total noise. If these two factors are considered, plus $\langle i_N \rangle = 0$, Eq. (10) should be modified to

$$\mathrm{SNR}_{\mathrm{unbalanced}} = \frac{\alpha^2 P_R P_S}{\left(\frac{2k_B T}{R_L} + e\alpha P_R + \frac{(1+V^2)}{3\Delta v}\alpha^2 (P_R + P_S)^2\right) B}. \quad (21a)$$

For balanced detection, the first two items in Eq. (1) will be eliminated during the process of differential amplification, so only the beat frequency noise exists in the overall redundancy intensity noise. As such, the system SNR becomes

$$\mathrm{SNR}_{\mathrm{balanced}} = \frac{\alpha^2 P_R P_S}{\left(\frac{2k_B T}{R_L} + e\alpha P_R + \frac{2(1+V^2)}{3\Delta v}\alpha^2 P_R P_S\right) B}. \quad (21b)$$

By comparing Eq. (21b) with Eq. (21a), one can see that the SNR of balanced detection is larger than that of unbalanced detection. In particular, suppose

$$\mathrm{SNR}_{\mathrm{balanced}} = \frac{1}{A}, \quad (22a)$$

then

$$\mathrm{SNR}_{\mathrm{unbalanced}} = \frac{1}{A+D}. \quad (22b)$$

Here, A is the reciprocal of Eq. (21b) and D is given by

$$D = \frac{\alpha^2 B(1+V^2)(P_R^2 + P_S^2)}{3\Delta v \alpha^2 P_R P_S}. \quad (22c)$$

Obviously,

$$\frac{\mathrm{SNR}_{\mathrm{balanced}}}{\mathrm{SNR}_{\mathrm{unbalanced}}} = 1 + \frac{D}{A}. \quad (23)$$

The superiority of balanced detection is thus determined by the value of D/A. It is clear that if the noise of the detector is relatively high, namely, A is large, the improvement of system SNR by balanced detection will not be obvious; on the other hand, if the noise of the detector is minimal, i.e., A is small, the balanced detection may improve the system SNR significantly.

When $\langle i_N \rangle \neq 0$ and $\langle i_N \rangle \gg \langle i_S \rangle$, that means stray light noise is high enough to submerge the signal light, the denominators of Eqs. (21a) and (21b) should be changed by replacing P_S with P_N. Therefore, in non-ideal situations, the respective SNR of OCT systems with unbalanced and balanced detection can be described by

$$\mathrm{SNR}_{\mathrm{unbalanced}} = \frac{\alpha^2 P_R P_S}{\left(\frac{2k_B T}{R_L} + e\alpha(P_R + P_N) + \frac{(1+V^2)}{3\Delta v}\alpha^2 (P_R + P_N)^2\right) B}, \quad (24a)$$

$$\mathrm{SNR}_{\mathrm{balanced}} = \frac{\alpha^2 P_R P_S}{\left(\frac{2k_B T}{R_L} + e\alpha(P_R + P_N) + \frac{2(1+V^2)}{3\Delta v}\alpha^2 P_R P_N\right) B}. \quad (24b)$$

From the above two equations, it can be seen that at either the limit of shot noise or the limit of thermal noise, there is almost no difference between balanced and unbalanced detections. It should be noted that because of the existence of stray light, the detectable minimum signal power at the shot noise limit will not be determined by Eq. (17), instead, it is given by

$$(P_S)_{\min} = \frac{h\nu B}{\eta}\left(1 + \frac{P_N}{P_R}\right). \quad (25)$$

Comparing Eq. (25) with Eq. (17), we can see that a modification factor is added, which is the ratio of the stray light power to the reference light power. An apparent conclusion that may be drawn from Eq. (25) is: the stray light in the system should be reduced as much as possible in order to improve the sensitivity of an OCT system. The stray light includes all of the parasitic reflections and the scattered light not from the detected sample. Details about how to relate the power of stray light with the optical parameters of a real-world OCT system and further discussions about Eqs. (24a) and (24b) can be found in Refs. [15] and [16].

5.4 Speckle noise

Optical speckles are caused by coherent addition of monochromatic light or quasi-monochromatic light with

random phases, and they are often observed as irregular spots on interference patterns. The intensity of the alternating light signal detected by the OCT detector is the coherent addition of the back-scattered sample light wave and the reference light wave. Here, the sample light wave is the summation of all the scattered wavelets within the coherent zone. These wavelets have random phases because of the random distribution of the scattering points and/or the fluctuation of the refractive index in the sample, which further leads to the speckle noise in the interference signal. Different from other types of noise, speckle noise is coherent noise.

According to the discussions given in Sect. 3, the carrier frequency of the interference signal in an ideal OCT system is given by $f_0 = 2V_R/\lambda_0$ (λ_0 is the central wavelength of the light source, V_R is the scanning velocity of the reference mirror). Similarly, the mean modulation frequency caused by speckles will be $f_{speckle} = 2V_R/l_C$, and l_C is the coherence length of the incidence light. If $l_C \gg \lambda_0$, the interference noise signal caused by speckles will be a low frequency signal. In such cases, fluctuation of the OCT signal directly associated with speckles can be eliminated or reduced by frequency filtering. However, for an OCT system with high longitudinal resolution we may have $l_C \approx \lambda_0$, so the frequency of speckle noise will be close to that of the useful interference signal from the two arms. Apparently, in this case, a bandpass filter circuit will unlikely reduce the speckle noise. In general, depending on the structure and the composition of the sample, a certain amount of speckle noise is always present in the interference signal of an OCT system.

Speckle noise can be treated as a special type of stray light noise, which is created only by the scattering points within the coherent volume surrounding a point signal source inside the sample. Like the effect of other kinds of noise, the presence of speckle noise within the frequency bandwidth of the real signal will reduce the sensitivity of an OCT system. In addition, speckle noise may modulate the longitudinal point spread function and in turn affect the longitudinal resolution of the OCT system. The impact of speckle noise on the interference signal along the direction of the optical axis can be described by a totally random initial phase α_{SR} in Eq. (1). In this way, the interference signal is turned into a random statistical signal that obeys Rayleigh distribution [3]. Consequently, in the worst scenario, the contrast of the interference signal would equal to 0.52, i.e., a corresponding SNR of 2.8 dB. In actual OCT systems, depending on the convergence and the spot size of the detection light within the sample, the space filtering effect of the effective numerical aperture may partially limit the speckle noise from entering the optical detector. Moreover, the depolarization effect of the scattering process may also reduce the amplitude of the speckle noise. The most effective way to eliminate speckle noise is to average the measured OCT interference signal by many times [17].

6 Analysis of signal-to-noise ratio for frequency-domain OCT systems

Frequency-domain OCT or also referred to as Fourier-domain OCT techniques have received much attention in recent years. FD-OCT employs a spectral discrimination approach and Fourier transformation to obtain the depth information of samples. The SNR of this spectrally discriminated technique is independent of the coherent length of the light source and the bandwidth of the detector, whereas the SNR of TD-OCT has an inverse relationship to the axial resolution and the signal frequency. In addition, FD-OCT does not need the relatively complicated fast scanning optical delay line. Recent results demonstrated that even in situations of weak signal power and high signal acquisition speed, sensitivities well above 100 dB could be achieved for a FD-OCT system [12,18]. We believe that FD-OCT with high resolution, high sensitivity, and high speed is likely to become a powerful diagnostic method for clinical applications.

Two different types of FD-OCT have been developed, namely, the spectral-domain OCT (SD-OCT) [12,19] and the swept-source OCT (SS-OCT) or optical frequency-domain imaging (OFDI) [18,20]. As shown in Fig. 1(b), in SD-OCT, individual spectral components of low coherent light are detected separately by using a spectrometer and a charge-coupled device (CCD) array. SS-OCT uses a wavelength-swept laser source and a conventional photodetector, and it is based on optical frequency-domain reflectometry for imaging. SS-OCT is particularly important for imaging in the 1300–1500 nm wavelength range, where low-cost array detectors are not available. Use of a wavelength-swept laser source for OCT imaging also makes it possible for balanced detection, which cannot be realized in SD-OCT. We believe that the advantages of SS-OCT will further enhance the performance of an OCT system in terms of image quality, speed and robustness. This section is devoted to a detailed discussion of signal-to-noise ratio in FD-OCT including SD-OCT and SS-OCT.

In an FD-OCT system, a photo-detector or a CCD array measures optical intensity as a function of wavelength of the interferometric signal from the sample and reference arms. In order to apply the discrete Fourier transform (DFT) for reconstructing the axial scan along Z axis, the spectrum should be sampled in the conjugate space, i.e., the wave number k space. The signal detected by the ith pixel as a function of k_m is given by

$$S_i(k_m) = \frac{1}{2}\alpha\rho(k_m)\left[R_R + R_S + 2\sqrt{R_R R_S}\cos(k_m\Delta l + \varphi_i)\right], \tag{26}$$

where α is the responsivity of the detector, $\rho(k_m)$ is the spectral density of the light source, R_R, R_S are the reference and sample arm reflectivities respectively, Δl is the path-length difference between the two arms, and φ_i

is the interferometeric phase shift. In ideal cases, even sampling in k space is required, i.e., the sampling step $\delta k = \Delta k/M$, with M as the integer number and Δk as the source bandwidth expressed in k space. It is easy to show that $\Delta k = 2\pi\Delta\lambda/\lambda_0^2$, where λ_0 is the central wavelength and $\Delta\lambda$ is the spectral bandwidth in wavelength. Obviously, we have sampling index number $m \in \{1, M\}$ in Eq. (26). The signal reflectivity as a function of depth, or $S(Z_n)$, can be obtained by making DFT of Eq. (26), which is

$$S(Z_n) = \sum_{m=1}^{M} S_i(k_m) \exp(-\mathrm{j}k_m Z_n). \tag{27}$$

The pixel spacing and the maximum scan depth in the Z-domain are given by $\delta z = \pi/\Delta k$ and $\Delta Z_{\max} = \pi/\delta k$. The scan depth, which is essentially from $-\pi/(2\delta k)$ to $+\pi/(2\delta k)$, can also be expressed as $\Delta Z_{\max} = \lambda_0^2/(2\delta\lambda)$, where $\delta\lambda$ is the sampling interval in wavelength. Thus, the image depth of a FD-OCT system is proportional to the square of the central wavelength of the light source, and inversely proportional to the wavelength sampling interval.

Since $S_i(k_m)$ is a real function, $S(+Z)$ and $S(-Z)$ in Eq. (27) actually form a pair of complex conjugates. The effective scan depth thus reduces to the half of $\lambda_0^2/(2\delta\lambda)$, i.e., $\Delta Z_{\max} = \lambda_0^2/(4\delta\lambda)$. If a complex signal is used, a full range of scan depth can be achieved. The design formula for determining the sampling number is given by $M = 2\Delta Z_{\max}\Delta k/\pi$. Besides the time needed for performing DFT, the equivalent A-scan speed will be determined by the integration time of the CCD array for SD-OCT, and the wavelength swept cycle time for SS-OCT. For a Gaussian source with a FWHM bandwidth Δk, the longitudinal or A-scan axial resolution can be expressed as $4\ln 2/\Delta k$, which is the same as that for time-domain OCTs.

For simplicity, let us consider the case of a single reflector located at $\Delta Z = n\lambda_m$ (n is an integer) acting as a sample. The peak value of the interferometric portion of the A-scan derived from Eqs. (26) and (27) is

$$S(\Delta Z) = \alpha\sqrt{R_R R_S}\sum_{m=1}^{M}\rho(k_m) = \alpha\sqrt{R_R R_S}S_{\mathrm{FD-OCT}}, \tag{28}$$

where $S_{\text{FD-OCT}}$ is the summation of the spectral density $\rho(k_m)$ over all m. Therefore, Eq. (28) can be regarded as the coherent summation of M waves of amplitude $\alpha\sqrt{R_R R_S}\rho(k_m)$.

In order to calculate the SNR of FD-OCT, we must transform the noise from the k space to the Z-domain. For $S_i(k_m)$ given by Eq. (26), a Gaussian white noise term can be introduced, which has a mean photocurrent of zero, a standard deviation $\sigma(k_m)$. In OCT systems, it is typical for $R_R \gg R_S$, thus, under the shot noise limit, $\sigma(k_m) = \sqrt{2eS_i(k_m)B_{\mathrm{FD-OCT}}}$, where e is the electronic charge and $B_{\text{FD-OCT}}$ is the noise equivalent bandwidth of the system [21]. In contrast to Eq. (28), the standard deviation of white noise at position z, σ_z, in Z space, is equal to the incoherent addition of M noise sources in k-domain as

$$\sigma_z = \sqrt{\sum_{m=1}^{M}\sigma^2(k_m)} = \sqrt{2e\alpha R_R S_{\mathrm{FD-OCT}}B_{\mathrm{FD-OCT}}}. \tag{29}$$

Thus, the SNR of FD-OCT is

$$\mathrm{SNR}_{\mathrm{FD-OCT}} = \frac{S^2(Z_n)}{\sigma_z^2} = \frac{\alpha R_S S_{\mathrm{FD-OCT}}}{2eB_{\mathrm{FD-OCT}}}. \tag{30}$$

By comparing Eq. (30) with the corresponding result of TD-OCT in Eq. (12), and considering $P_S = R_S S_{\text{TD-OCT}}$, as well as in the case of a Gaussian source we also have $S_{\text{FD-OCT}} = (1/2)MS_{\text{TD-OCT}}$, $B_{\text{FD-OCT}} = B_{\text{TD-OCT}}$ [21,22], we get

$$\mathrm{SNR}_{\mathrm{FD-OCT}} = \frac{M}{4}\mathrm{SNR}_{\mathrm{TD-OCT}}. \tag{31}$$

Equation (31) indicates that as long as $M > 4$, the SNR of FD-OCT will be higher than that of TD-OCT. At first glance, compared with the case in TD-OCTs, the signal intensity at each pixel of a linear array detector of an FD-OCT is reduced by M times on average, whereas the frequency bandwidth or the noise is also reduced by M times, therefore, the overall noise at each pixel should make no difference for either frequency-domain or time-domain OCTs. However, for FD-OCTs, making Fourier transform involves the summation of all the signals at different frequencies, and such a summation is a coherent addition for signal, but incoherent or intensity addition for noise, namely, the noise is added to M times but the signal is added to M^2 times. Because the optical density in Z space after Fourier transform is distributed evenly on both sides of the zero point, the eventual SNR of an FD-OCT system is $M/2$ times higher than that of a TD-OCT system. For light sources of non square-shaped spectrum, the effective frequency bandwidth will be less than M times the bandwidth of the signal on each detector pixel. In this case, SNR of an FD-OCT should be multiplied by a spectral shape factor, which is 0.5 for a Gaussian-shaped spectral profile. $\mathrm{SNR}_{\text{FD-OCT}}/\mathrm{SNR}_{\text{TD-OCT}}$ or $M/4$ may be regarded as the SNR advantage of FD-OCT over TD-OCT. From Eq. (31), we know that the SNR advantage of FD-OCT over TD-OCT is independent of source bandwidth and scan depth.

In Fig. 4 the relationship between A-scan depth and the source bandwidth associated with five sets of different sampling numbers M and SNR advantage values g are present. For example, when $M = 2000$, 27 dB SNR advantage of FD-OCT over TD-OCT is obtained and its A-scan depth is two times more than that when $M = 1000$. These data are calculated using Eqs. (26)–

(31) for a Gaussian source centered at 1500 nm. SNR advantage is defined as $g = \mathrm{SNR}_{\mathrm{FD\text{-}OCT}}/\mathrm{SNR}_{\mathrm{TD\text{-}OCT}}$ expressed in dB.

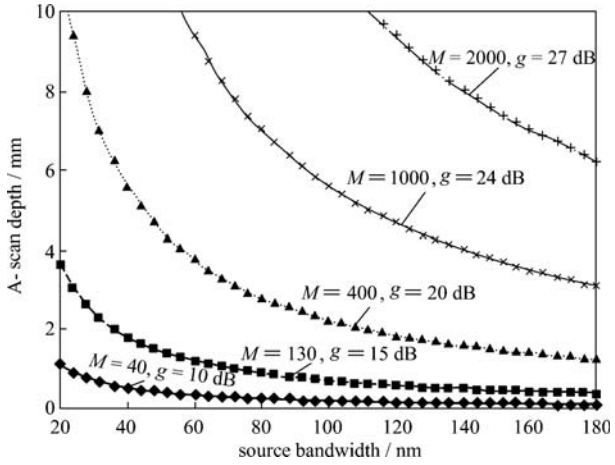

Fig. 4 Relationship between A-scan depth and source bandwidth for different wavelength sampling number M and SNR advantage of FD-OCT over conventional TD-OCT

The SNR of FD-OCT may be expressed in a more general form for shot noise limited systems [19] as

$$\mathrm{SNR}_{\mathrm{FD-OCT}} = \frac{\eta P_{\mathrm{S}}}{h\nu_0 f_{\mathrm{A}}}, \tag{32}$$

where f_{A} is the A-scan rate. Equation (32) tells us that the effective detection bandwidth in FD-OCT is equal to the A-scan rate instead of the detector bandwidth. Based on the same principle as that used above to derive the sensitivity for TD-OCT systems, the sensitivity of FD-OCT defined as the minimum detectable signal power can be expressed as

$$\beta_{\mathrm{sensitivity(FD-OCT)}} \equiv P_{\mathrm{S(min)}} = \frac{h\nu_0 f_{\mathrm{A}}}{\eta}. \tag{33}$$

For a numerical example, assuming a FD-OCT system has a video image rate of 30 frame/s, and its lateral sampling point is 500, the A-scan rate required is 15 kHz, and the sensitivity of the FD-OCT system calculated from Eq. (33) is 0.3×10^{-14} W. As a comparison, in a TD-OCT system with the same imaging rate and a detector bandwidth Δf of 5 MHz, the sensitivity calculated from Eq. (17) is 100×10^{-14} W. Apparently, under the same video image rate, the sensitivity of the FD-OCT system is 300 times (25 dB) higher than that of the TD-OCT system. An ultra-fast SS-OCT system with 370 kHz A-scan speed and 370 frame/s image rate was recently reported [23]. Such a result clearly indicates that SS-OCT is a promising technique for three-dimensional (3D) real-time clinical diagnosis applications.

7 Conclusions

In summary, in order to successfully design and develop high performance optical coherence tomography systems, the fundamental theories of system noise analyses for both time-domain and frequency-domain OCT systems are presented. By comparative study of the noise limits that could exist for ideal OCT systems and the influences of both balanced and non-balanced detection schemes on the characteristics of the system noise, and also by the noise calculation of both time-domain and frequency-domain OCTs, as well as the effect of stray light (including speckle noise) on the dynamic range, we can draw the following conclusions:

1) Because of the detection of the dual beam interference signal, the noise equivalent power of an OCT system is halved compared with the direct single beam detection. The SNR of an OCT system may be adjusted through controlling the optical power of the reference beam.

2) In order to make an OCT system operate at the shot noise limit and with the maximum dynamic range, it is imperative to use low noise optoelectronic detectors with high saturation intensity. For the scheme of balanced detection, the main characteristics of the two detectors should be as close as possible.

3) In practice, whether an OCT system operates at the shot noise limit may be verified by the trend of SNR variation versus the optical power of the reference beam.

4) For those time-domain OCT systems that do not operate at the shot noise limit, the optimum SNR can be obtained through properly selecting the optical power of the reference beam. Such an optimum optical power of the reference beam is associated with the point where the redundant intensity noise equals the thermal noise of the detector, and is independent of the optical power of the signal beam.

5) Under the shot noise limit, the signal-to-noise ratio of a time-domain OCT system is inversely proportional to the image acquisition speed, but proportional to the coherence length of the light source, which means in this case optimum SNR and high longitudinal resolution cannot be achieved simultaneously. A tradeoff between these two parameters must be considered in system design.

6) For actual OCT systems, the presence of all kinds of stray light can lead to the decrease of system SNR. Thus, in order to increase the sensitivity of an OCT system, one must minimize the stray light within the system.

7) Being a type of coherent noise, optical speckles are strongly dependent on both the structure and constitution of the sample. In general, speckle noise cannot be filtered out completely by the coherence gate. Speckle noise may induce large modulations on the longitudinal point spread function and thus lower down the longitudinal resolution of the OCT system. An effective way to suppress speckle noise is making repetitive measurements and then averaging the results.

8) Different from that in time-domain OCT systems, the SNR of frequency-domain OCT systems does not depend

on the bandwidth of the light source or the depth of the longitudinal scan. Therefore, a frequency-domain OCT system usually can maintain a large dynamic range even under situations of high speed image acquisition.

Finally, it must be pointed out that all we have discussed in this paper is actually only on the noise of an OCT system with physical origins. The noise arising from digitization in the image acquisition process and the techniques of noise reduction using background subtraction or filtering have not been included. These shall be covered by the topics of our future studies.

Acknowledgements This research was supported by the State Key Program of National Natural Science Foundation of China (Grant No. 60637020) and the National Natural Science Foundation of China (Grant No. 60677012).

References

1. Huang D, Swanson E A, Lin C P, et al. Optical coherence tomography. Science, 1991, 254(5035): 1178–1181
2. Schmitt J M. Optical Coherence Tomography (OCT): a review. IEEE Journal of Selected Topics in Quantum Electronics, 1999, 5(4): 1205–1215
3. Fercher A F, Drexler W, Hitzenberger C K, et al. Optical coherence tomography - principles and applications. Reports on Progress in Physics, 2003, 66(2): 239–303
4. De Boer J F, Milner T E, Van Gemert M J C, et al. Two-dimensional birefringence imaging in biological tissue by polarization-sensitive optical coherence tomography. Optics Letters, 1997, 22(12): 934–936
5. Oh J-T, Kim S-W. Polarization-sensitive optical coherence tomography for photoelasticity testing of glass/epoxy composites. Optics Express, 2003, 11(14): 1669–1676
6. Chen Z P, Milner T E, Dave D, et al. Optical Doppler tomographic imaging of fluid flow velocity in highly scattering media. Optics Letters, 1997, 22(1): 64–66
7. Chen Z P, Milner T E, Srinivas S, et al. Noninvasive imaging of *in vivo* blood flow velocity using optical Doppler tomography. Optics Letters, 1997, 22(14): 1119–1121
8. Schmitt J M, Xiang S H, Yung K M. Differential absorption imaging with optical coherence tomography. Journal of the Optical Society of American A, 1998, 15(9): 2288–2296
9. Wojtkowski M, Bajraszewski T, Targowski P, et al. Real-time *in vivo* imaging by high-speed spectral optical coherence tomography. Optics Letters, 2003, 28(19): 1745–1747
10. Jia Y Q, Liang Y M, Mu G G, et al. Analysis of fast scanning system in optical coherence tomography. Chinese Journal of Laser Medicine & Surgery, 2006, 15(1): 62–65 (in Chinese)
11. Leitgeb R, Hitzenberger C K, Fercher A F. Performance of Fourier domain vs. time domain optical coherence tomography. Optics Express, 2003, 11(8): 889–894
12. Yun S H, Tearney G J, Bouma B E, et al. High-speed spectral-domain optical coherence tomography at 1.3 μm wavelength. Optics Express, 2003, 11(26): 3598–3604
13. Mansuripur M. The Physical Principles of Magneto-optical Recording. London: Cambridge University Press, 1998, 295–306
14. Rollins A M, Izatt J A. Optimal interferometer designs for optical coherence tomography. Optics Letters, 1999, 24(21): 1484–1486
15. Podoleanu A G. Unbalanced versus balanced operation in an optical coherence tomography system. Applied Optics, 2000, 39(1): 173–182
16. Takada K. Noise in optical low-coherence reflectometry. IEEE Journal of Quantum Electronics, 1998, 34(7): 1098–1108
17. Schmitt J M, Xiang S H, Yung K M. Speckle in optical coherence tomography. Journal of Biomedical Optics, 1999, 4(1): 95–105
18. Yun S H, Tearney G J, De Boer J F, et al. High-speed optical frequency-domain imaging. Optics Express, 2003, 11(22): 2953–2963
19. Nassif N A, Cense B, Park B H, et al. *In vivo* high-resolution video-rate spectral-domain optical coherence tomography of the human retina and optic nerve. Optics Express, 2004, 12(3): 367–376
20. Wojtkowski M, Srinivasan V J, Ko T H, et al. Ultrahigh-resolution, high-speed, Fourier domain optical coherence tomography and methods for dispersion compensation. Optics Express, 2004, 12(11): 2404–2422
21. Choma M A, Sarunic M V, Yang C, et al. Sensitivity advantage of swept source and Fourier domain optical coherence tomography. Optics Express, 2003, 11(18): 2183–2189
22. De Boer J F, Cense B, Park B H, et al. Improved signal-to-noise ratio in spectral-domain compared with time-domain optical coherence tomography. Optics Letters, 2003, 28(21): 2067–2069
23. Huber R, Adler D C, Fujimoto J G. Buffered Fourier domain mode locking: unidirectional swept laser sources for optical coherence tomography imaging at 370,000 lines/s. Optics Letters, 2006, 31(20): 2975–2977